(Article begins on next page)

A Charge-Integrated Modular NIR Armband for Forearm Optical Myography

Giovanni Gibertoni*†, Alberto Besozzi*, Luigi Rovati*
*Department of Engineering "Enzo Ferrari", University of Modena and Reggio Emilia, Italy
†Department of Biomedical, Metabolic and Neural Sciences, University of Modena and Reggio Emilia, Italy

***Abstract*—Optical myography is a promising wearable alternative to surface electromyography. However, existing implementations are often constrained by reflective sensor modules and transimpedance-based analog front ends, which limit scalability, dynamic range, and mechanical integration. This paper presents a modular near-infrared (NIR) armband for optical myography of the forearm based on discrete high-power 850 nm LEDs, silicon PIN photodiodes, and charge-integration digitization. The device performs a complete emitter–detector sweep to obtain a multichannel measurement map at 5 Hz, with distance-dependent integration and illumination timing to extend dynamic range while limiting optical cross-talk.**

A dataset of 50,587 balanced windows from four subjects performing four gestures in two forearm postures across multiple sessions was collected. A hard-gated multi-task CNN decouples posture recognition from gesture decoding via posture-specific experts. Mixed-subject evaluation achieved 92.5% $\pm$ 4.6% gesture accuracy with near-perfect posture recognition. Session-to-session placement variability caused marked performance degradation, which was effectively mitigated through few-shot transfer learning, enabling rapid adaptation with minimal calibration, including for previously unseen users. These results support modular NIR sensing with charge integration as a practical pathway toward robust, low-profile forearm interfaces for daily-use gesture recognition.

***Index Terms*—Optical myography, near-infrared sensing, wearable sensors, gesture recognition, charge integration**

I. Introduction

Myography refers to a range of techniques used to quantify muscular activity [1]. The most common approach is surface electromyography (sEMG), which non-invasively captures the electrical signals produced by muscle fibers at the skin surface [2]. For upper-limb musculature, sEMG is extensively used for the recognition and analysis of arm movements, supporting applications such as motion tracking, human–machine interaction, and myoelectric control. Nonetheless, its reliability is strongly affected by electrode positioning, contact quality, skin impedance variability, and motion artifacts, all of which can undermine robustness in real-world environments [3], [4], [5], [6].

Conventional myoelectric control systems employ handcrafted feature extraction and pattern recognition for gesture decoding and have been investigated for many decades [7]. Wrist-mounted sEMG has recently attracted particular interest because it can be embedded into common wearable devices. Comparative studies of wrist versus forearm sEMG indicate that wrist recordings can yield superior signal and information quality for fine finger movements while preserving similar performance for wrist gestures [8]. Furthermore, deep learning methods enhance wrist-based decoding and can surpass traditional pipelines when signals are collected at the wrist [9]. However, ensuring robustness to inter-session variability and changes in limb posture remains a key obstacle for deployment in everyday settings [10], [11].

To mitigate the limitations of conventional electromyography, alternative approaches such as sonomyography, Force Myography (FMG), and optical myography (OMG) have been explored to capture muscle activity through different physical transduction mechanisms, each with distinct advantages and limitations in terms of signal quality, hardware complexity, device positioning, and user comfort.

Sonomyography uses ultrasound images to infer muscle activity and provides rich spatial information regarding deep muscle architecture, demonstrating high accuracy for hand gesture recognition and functional task performance in prosthetic control [12], [13]. Despite its strong potential, practical barriers such as the requirement for bulky probes, acoustic coupling media, probe stability, ergonomics, and translation to low-profile wearable systems often hinder seamless wearable integration [14], [15]. These constraints motivate alternative sensing solutions that preserve wearability while retaining discriminative information.

A mechanically robust alternative is FMG, which leverages arrays of pressure or force sensors placed circumferentially around the forearm. FMG captures the volumetric expansion and stiffness changes of underlying muscles during contraction [16], [17]. Innovations in this field include the use of optical fiber sensors to detect mechanical deformation with high sensitivity [18], [19]. These approaches offer inherent immunity to electrical noise and skin impedance variations, although they remain sensitive to tightness and sensor shifting.

More recently, OMG has emerged as a promising domain, initially implemented through computer vision techniques. These imaging-based approaches use external cameras to monitor the forearm surface and extract features such as skin deformation, contour shifts, and superficial venous patterns, which are typically processed using deep learning for hand gesture recognition [20], [21]. While effective in controlled environments, camera-based solutions often struggle with ambient lighting variability, occlusion, and form-factor constraints, which limit their robustness in daily life use.

To enhance portability and robustness, Near-Infrared (NIR) optical sensing provides a practical alternative to camera-based OMG by using surface-mounted emitter–detector measurements that are less affected by ambient light and can be positioned towards the elbow. In soft biological tissue, photon propagation in the NIR range is dominated by scattering, while absorption and penetration depth vary strongly with wavelength [22], [23]. With source–detector (S–D) pairs on the skin, NIR light probes subsurface tissue and captures changes in optical coupling and photon paths caused by forearm muscle deformation and tendon motion [24]. Gesture-induced changes in tissue geometry and optical path length appear as intensity variations. Muscle activation and tendon movement alter local morphology and boundary conditions, producing a rich, high-dimensional optical signature well suited to learning-based analysis.

This work introduces a modular NIR armband engineered to acquire dense spatiotemporal optical maps at the mid-forearm level. The device integrates high-power NIR emitters and photodiodes into a TPU-based enclosure, enabling stable skin contact. The proposed architecture features circular, multi-channel integrated-light acquisition that avoids conventional transimpedance amplifier (TIA) front-ends while enabling digital control of sensitivity, dynamic range, and optical crosstalk as a function of source–detector distance. This design enables scalable sensor density, yields extensive cross-channel information, and supports a compact, practical forearm interface that converts complex optical measurements into reliable gesture recognition, maintaining consistent performance despite wearing variations.

II. Related Work

The development of optical methods for muscle activity recognition has progressed from foundational investigations into Near-Infrared Spectroscopy (NIRS) for prosthetic control [25] to multimodal systems that integrate optical sensing with surface electromyography (sEMG) to improve gesture decoding accuracy [26], [27]. Despite the promise of these techniques, existing wearable solutions are often constrained by their underlying hardware architectures. Many implementations rely on pre-packaged reflective sensors, such as the RPR-220, which require a specific focal distance to maintain sensitivity, thereby imposing mechanical design limitations that hinder low-profile integration [28]. Furthermore, traditional acquisition chains typically employ phototransistors and TIA to convert instantaneous photocurrent into voltage [29], [30]. These TIA-based designs increase electronic complexity, necessitate careful noise and bandwidth management, and often suffer from fixed gain characteristics that limit adaptability to different forearm sizes or tissue compositions.

Recent efforts have explored denser sensor arrays and infrared-based bracelets to decode complex hand gestures [24], [31]. However, these systems often prioritize localized sensing strategies, where each detector primarily captures light from an adjacent emitter, limiting the exploitation of cross-channel interactions. Since light penetration depth and fluence distribution are strongly dependent on wavelength and source–detector geometry [22], [23], capturing deeper and more global biomechanical changes requires a more comprehensive sensing strategy.

Unlike prior architectures, this work adopts discrete LED–photodiode pairs with charge integration over a configurable time window. Temporal integration of the optical signal enhances sensitivity to weak signals while inherently averaging electronic noise. This simplifies the front-end electronics and allows digital tuning of optical excitation and integration settings for each S–D pair. Consequently, the system adjusts its dynamic range to varying forearm geometries and tissue properties while preserving a compact hardware implementation.

III. Materials and Methods

A. System overview

The proposed wearable system is a modular NIR optical armband designed to acquire circular measurements of light propagation within the forearm tissue. The device consists of a compliant ring of discrete sensing modules fabricated in TPU using commercial fused deposition modeling (FDM) 3D printing, conforming to the arm surface (Figure 1). The current prototype implements eight identical emitter–receiver modules uniformly distributed around the forearm circumference.

Each module integrates one high-power NIR LED emitter and one silicon PIN photodiode, ensuring repeatable placement and stable optical coupling with the skin (Figure 1c). The modular mechanical and electrical design supports configurations from 2 to 8 active modules without changes to the acquisition electronics. Short-separation pairs are primarily sensitive to superficial back-scattered photons, whereas larger separations probe deeper tissue volumes through longer, multiply scattered photon trajectories.

The system adopts 850 nm surface-emitter LEDs (Vishay VSMA1085750X02) and silicon PIN photodiodes with a daylight-blocking filter (Vishay VBP104FAS). A narrow-bandpass optical filter centered at the emitter wavelength is mounted on each photodiode to further suppress ambient illumination.

During operation, a single LED emitter is activated at a time, while all others remain off, to minimize optical crosstalk and instantaneous power consumption. The driver uses an 8-channel power shift register (Texas Instruments TLC6A598), while the photodiode currents are routed through an 8:1 analog multiplexer (MAX4617) into a compact signal-conversion chain. Photocurrents are digitized using a dual current-input, 20-bit charge-integration ADC (Texas Instruments DDC112), well suited for low currents due to noise averaging over the integration window and programmable dynamic range via integration time and feedback capacitance selection. The acquisition board is controlled by an Arduino UNO R4 microcontroller that manages LED sequencing, multiplexer selection, DDC112 timing/readout, and data streaming.

B. Signal Acquisition

Each scan consists of an emitter–receiver sweep that produces an 8×8 measurement map. For each photodiode ($i \in$

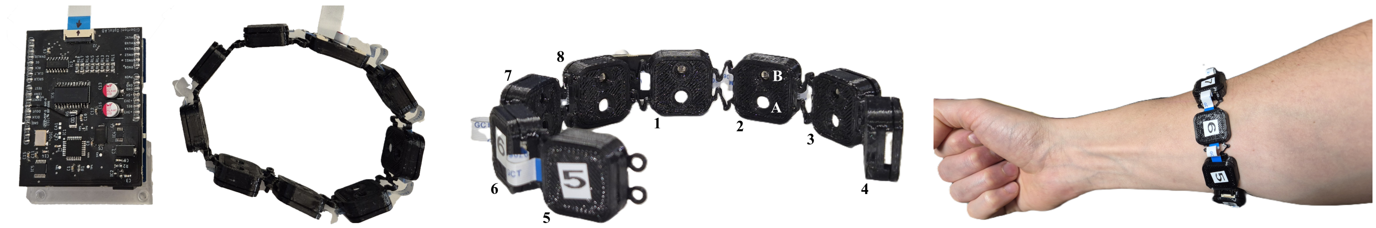

(a) (b) (c)

Fig. 1: Device prototype realized in this study. (a) Assembled TPU armband connected to the microcontroller acquisition board. (b) Details of the TPU bracelet, composed of 8 identical optical modules, where 'A' indicates the photodiode, and 'B' denotes the NIR LED emitter. (c) The armband worn around the forearm.

$\{1,\ldots,8\}$), all eight LEDs ($j \in \{1,\ldots,8\}$) are sequentially enabled and sampled, yielding 64 readings in PD-major order.

A deterministic scheduler drives the DDC112 conversion control (CONV) and uses a data-valid interrupt to retrieve each conversion with minimal jitter. Because attenuation increases with S–D separation, the firmware selects the photodiode integration time and LED turn-on duration as functions of the active S–D pair distance. This improves dynamic range while preventing saturation on short paths.

The $i = j$ pairs are excluded from active measurements because these signals saturate even at the minimum integration time ($T_{int} = 500\,\mu$s, set to maintain the DDC in continuous mode without overflow) and minimum LED on-time ($T_{on} = 20\,\mu$s). Instead, these pairs are used as dark measurements (all LEDs turned off), thus indicating the ambient light level. LED activation is synchronized with the onset of the integration window, whereas turn-off is enforced before the end of the integration period. This timing ensures that the LED fully deactivates before the onset of the next integration cycle, thereby mitigating optical crosstalk. The specific T_{int} and T_{on} for each (i, j) S–D pair are described in Table I.

TABLE I: Integration times (T_{int}) and LED on-times (T_{on}) configured for different source–detector distances (d). Distance is defined as the minimum number of steps between modules in the circular array.

Distance d	T_{int} (μs)	T_{on} (μs)
0	500	0
1	500	80
2	1000	700
3	2000	1700
4	4000	3700

Each acquisition is transmitted over a wireless link to a host system at a frequency of approximately five measurements per second ($f_s = 5$ Hz), where a Python-based user interface reconstructs the 8×8 map, renders a real-time heatmap visualization, and allows the recording of labeled datasets together with associated metadata (gesture label, posture condition, and session identifier). The acquisition rate is matched to the quasi-static nature of light transport variations induced by sustained muscle activation and tissue deformation, rather than to rapid electrophysiological transients typically targeted by electromyography.

C. Dataset and Experimental Protocol

Data were acquired from four healthy male participants (age range: 22–48 years) following the hardware specifications described in Section III. Measurements were conducted in a controlled dark environment to isolate the optical contribution of the NIR emitters, maintaining a background dark signal below 0.5% of the 20-bit full-scale range.

Subjects were instructed to sit with the elbow resting on a desk and perform a predefined set of four gestures (Closed Fist, Open Hand, Thumb Up, and Index Finger Up). The bracelet was worn by sliding it toward the elbow and positioned approximately at mid-forearm, with minor subject-dependent variations in placement. Each gesture was held for 20 s, with a 3 s pause between consecutive gestures. The full gesture sequence was repeated eight times in both prone and supine forearm postures within the same macro-session, resulting in a total duration of approximately 12 min. Between consecutive macro-sessions, the armband was removed and re-mounted, and each acquisition was performed on a different day to introduce variability in sensor placement and forearm biomechanics.

Before segmentation, a data-cleaning stage removed samples affected by sensor readout errors, wireless transmission faults, or involuntary movements; these accounted for less than 3% of the total data. The remaining time-series were segmented into sliding windows of $T_{win} = 4$ s ($N = 20$ samples) with a step of one sample, retaining only windows containing a single ground-truth label.

The final dataset comprises 50,587 valid windows and is strictly balanced across the four gesture classes (Table II). Subjects P1 and P2 performed three macro-sessions on different days to capture inter-session variability, while subjects P3 and P4 performed a single session to assess inter-subject generalization. While the sample population size is limited, the goal of this study is not population-level benchmarking but the characterization of a novel optical sensing architecture.

All procedures were conducted in accordance with the Declaration of Helsinki, and all participants provided informed consent before data collection.

TABLE II: Dataset composition. The dataset is strictly balanced across the four gesture classes for all subjects.

Subject	Macro-sessions	Total Windows	Avg. per Class
P1	3	20,780	$\approx$ 5,195
P2	3	19,411	$\approx$ 4,850
P3	1	5,195	$\approx$ 1,300
P4	1	5,201	$\approx$ 1,300
Total	**8**	**50,587**	**-**

D. Machine Learning Network Architecture

Hand gesture recognition is performed using a custom Multi-Task Convolutional Neural Network (CNN) with a hard-gating mechanism, explicitly designed to decouple gesture classification from forearm posture (prone or supine).

The network processes a 64-dimensional input vector (one feature per LED–photodiode pair) through a shared feature-extraction backbone composed of stacked one-dimensional convolutional (Conv1D) layers with ReLU activations and global average pooling, yielding a compact latent representation of the spatiotemporal gesture patterns.

From this shared representation, the architecture branches into three heads:

1) **Posture classifier:** a fully connected branch that predicts the forearm posture ($y_{posture}$).
2) **Prone-specific expert:** a gesture classification head specialized for the *Prone* posture.
3) **Supine-specific expert:** a gesture classification head specialized for the *Supine* posture.

During inference, the predicted posture acts as a hard gate that selectively activates the corresponding gesture expert, implementing a context-driven Mixture-of-Experts scheme.

Training is performed end-to-end under a multi-task learning framework by minimizing a weighted sum of the gesture and posture cross-entropy losses:

$$L_{total} = L_{gesture} + \lambda \cdot L_{posture}. \tag{1}$$

E. Performance evaluation

The quantitative assessment of the proposed system relies on standard multi-class accuracy and confusion matrices to evaluate *Overall Classification Performance* across different gestures (Section IV-A). To rigorously test the robustness of the model against the primary sources of variance in optical myography (namely, inter-subject anatomical diversity and sensor repositioning) two distinct adaptation protocols were defined. First, an *Inter-Subject Adaptation* experiment is conducted to emulate a cold start condition for a previously unseen user; in this configuration, the network is pre-trained on a pool of historical subjects and evaluated on an excluded target subject. To mitigate the performance degradation caused by anatomical domain shifts, a transfer learning strategy is applied wherein the pre-trained weights are fine-tuned using an incrementally increasing subset of data from the target user (ranging from 100 to ≈ 3000 samples, corresponding to a maximum of three minutes of acquisition). This procedure allows for the reconstruction of a learning curve that quantifies the amount of calibration data required to reach optimal performance (Section IV-C). Second, an *Intra-Subject Adaptation* experiment is conducted to assess robustness against misplacement effects; in this case, the model is trained on previous sessions of a specific user and fine-tuned on a new session acquired on a different day, adopting the same incremental data injection strategy to measure the system's ability to recover accuracy despite variations in sensor placement and optical coupling (Section IV-B).

IV. Results and Discussion

This section evaluates the results of the proposed optical armband across different operating scenarios. Firstly, the overall performance is established using a mixed-subject protocol to validate the described architecture. Moreover, the critical challenges of wearable interfaces are addressed, specifically focusing on robustness to sensor repositioning (Intra-Subject Adaptation) and generalization to unseen users (Inter-Subject Adaptation).

A. Overall Classification Performance

To assess the intrinsic capability of the hardware to capture distinctive biomechanical patterns, the model was first evaluated in a mixed-subject configuration. Data from all users and sessions were pooled, using a Stratified Group K-Fold validation to prevent temporal leakage. The accuracy has been evaluated for each individual subject first for the posture of the forearm, and then for the gesture of the hand in prone position, supine position, and both.

To ensure the statistical reliability of the results and account for the stochastic nature of neural network weight initialization, the training procedure was repeated 10 times using different random seeds. The final performance metrics are reported as the mean $\pm$ standard deviation across these independent runs, providing a measure of the model's convergence stability.

As detailed in Table III, the system achieved an average gesture accuracy of $92.5\% \pm 4.6\%$ across the cohort, while individual performance varies slightly (P1 reached 96.5%, while P3 stood at 88.8%), the high aggregate score confirms that the 64-channel optical map captures sufficient information to distinguish fine gestures.

TABLE III: Mixed-Subject Classification Accuracy (%, Mean $\pm$ Std)

Subj.	Posture	Gesture Accuracy		
		All	Prone	Supine
P1	99.9 ± 0.1	96.5 ± 1.2	94.2 ± 1.8	98.9 ± 1.3
P2	100.0 ± 0.0	91.0 ± 1.6	88.7 ± 2.3	92.9 ± 2.3
P3	99.9 ± 0.2	88.8 ± 6.0	82.9 ± 8.9	94.6 ± 4.7
P4	100.0 ± 0.0	93.6 ± 3.6	91.3 ± 6.0	95.8 ± 2.6
Avg	$\mathbf{100.0 \pm 0.1}$	$\mathbf{92.5 \pm 4.6}$	$\mathbf{89.3 \pm 6.9}$	$\mathbf{95.5 \pm 3.7}$

Notably, the Posture Classifier branch delivered perfect performance ($\approx 100\%$ accuracy) for all subjects. This result is supported by the geometric variations produced by bone repositioning, which lead to substantial changes in light trajectories, as illustrated in Figure 2.

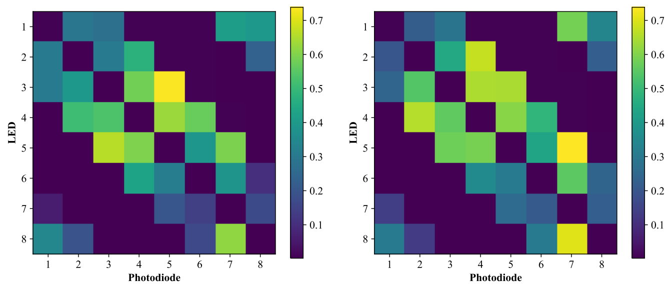

(a) (b)

Fig. 2: Spatial distribution of the optical signal averaged over all subjects. (a) Prone activation map. (b) Supine activation map.

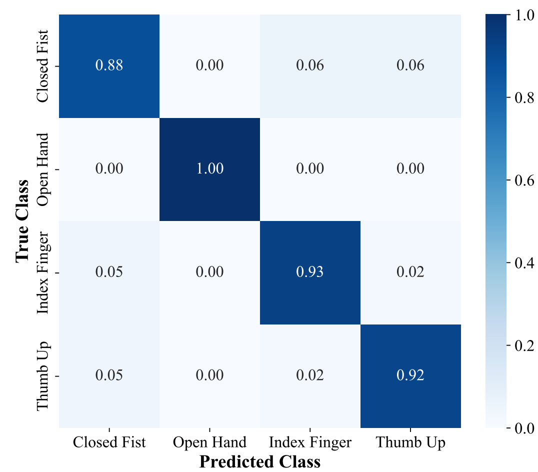

Fig. 3: Overall Confusion Matrix. The 'Open Hand' gesture is recognized accurately, whereas slight confusion remains between the flexor-controlled classes (Fist vs. Fingers) because of similar muscle activation patterns.

A closer inspection of the results reveals a consistent performance asymmetry between postural conditions: the system achieves higher accuracy in the *Supine* position ($95.5\% \pm 3.7\%$) compared to the *Prone* position ($89.3\% \pm 6.9\%$). This trend is observed across all subjects, with P3 showing the largest gap. This discrepancy can be attributed to biomechanical constraints. In pronation, the radius rotates over the ulna, inducing greater tension in the interosseous membrane and compressing the flexor and extensor compartments. This reduces the dynamic range of muscle displacement during fine finger movements, generating subtler optical variations compared to the more relaxed muscle distribution typical of the supine posture.

Another key observation concerns the class-wise performance. The *Open Hand* gesture achieves perfect classification accuracy (100%). From a biomechanical standpoint, this is expected, as it is the only gesture in the dataset primarily governed by the extensor compartment, which produces an optical signature that is clearly distinguishable from the flexor-dominant gestures. In contrast, most misclassifications arise from confusion between the *Closed Fist* gesture (88% accuracy) and the single-finger gestures (*Index*, *Thumb Up*). Specifically, 6% of the samples that should be classified as Closed Fist are erroneously predicted as Index Finger, and an additional 6% are misclassified as Thumb Up (see Figure 3). These confusions arise because the visual distinctions between these hand configurations are extremely subtle, making them difficult for the model to reliably separate.

Lastly, as depicted in Figure 2, S–D pairs separated by 3 or 4 modules exhibit very low light levels, even when long integration times are used (Table I). This behavior arises because it is inherently difficult for light to traverse the arm completely, and this difficulty is strongly influenced by the specific positioning of the bracelet on the forearm.

B. Intra-Subject Adaptation

In practical usage scenarios, removing and wearing the bracelet unavoidably causes spatial misalignment between the optical sensors and the targeted muscle compartments. To quantify this effect, the analysis leveraged the extended recordings from subjects P1 and P2 (Table II). Because each subject completed three macro sessions on different days, the evaluation has been executed as follows: the model was trained on the combined data from sessions S_1 and S_2 and tested on session S_3. This setup emulates a practical use case in which the system exploits prior calibration data to function on a subsequent day.

The results, summarized in Table IV, highlight the high spatial selectivity of the optical interface. Subject P1, who utilized skin markers to ensure precise sensor registration, maintained a high calibration-free generalization accuracy ($81.1\% \pm 3.3\%$). Conversely, subject P2, who relied on approximate visual alignment without fiducial markers, experienced a significant performance drop, with a cold start accuracy falling to $38.3\% \pm 4.5\%$. This discrepancy indicates that the dense optical scan is highly sensitive to centimeter-level displacements. While this sensitivity enables the detection of minute muscle deformations, it necessitates a compensation strategy for unconstrained usage.

TABLE IV: Calibration-Free Intra-Subject Performance (Train on $S_1, S_2 \rightarrow$ Test on S_3)

Subject	Placement Strategy	Acc. Gesture	Acc. Posture
P1	With Markers (Precise)	$81.1\% \pm 3.3\%$	$97.4\% \pm 4.0\%$
P2	No Markers (Approx.)	$38.3\% \pm 4.5\%$	$89.1\% \pm 3.8\%$

To recover performance in the presence of such replacement shifts, the proposed transfer learning strategy was applied. As illustrated in Figure 4, injecting a minimal calibration set from the new session is sufficient to realign the decision boundaries. For subject P2 (Figure 4b), accuracy recovered dramatically from the baseline of 38.3% to $84.7\% \pm 3.1\%$ using just 100 samples (approximately 20 seconds of data), effectively compensating for the misalignment. For P1 (Figure 4a), where cold start performance was already high due to marker usage (81.1%), the adaptation further refined the accuracy to $88.5\% \pm 1.0\%$.

Notably, posture recognition remained robust ($> 89\%$ for P2, $> 97\%$ for P1) in both scenarios before adaptation, confirming that macroscopic limb orientation features are preserved even under sensor displacement. These results suggest that the feature space learned from historical sessions is reusable, requiring only a short daily enrollment phase to adjust to the specific sensor-to-skin coupling.

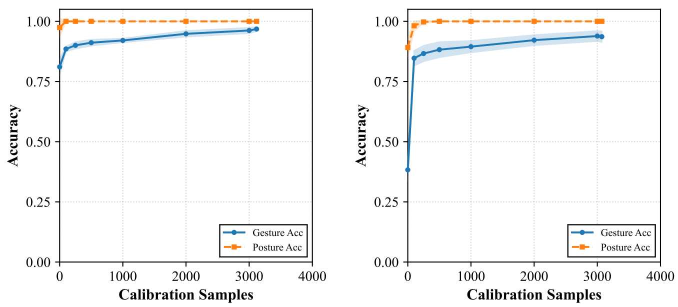

(a) (b)

Fig. 4: Intra-Subject Adaptation curves evaluated on a new session (S_3). (a) Subject P1 (With Markers) maintains high cold start accuracy. (b) Subject P2 (No Markers) exhibits a critical recovery with just 100 samples.

C. Inter-Subject Adaptation

The final stage of the evaluation examined how well the system generalizes to entirely new users. Specifically, a model trained beforehand on the source domain (subjects P1, P2) was applied to separate, held-out target subjects (P3, P4).

The calibration-free (direct transfer) performance on new targets yielded an average accuracy of approximately 36%. This baseline confirms that raw optical signatures are highly subject-specific, being heavily influenced by inter-subject anatomical variability such as limb circumference, subcutaneous fat thickness, and muscle depth. However, applying the proposed transfer learning protocol yielded substantial performance recovery, as detailed in Figure 5. Target subject P3 exhibited rapid feature alignment: accuracy rose to $68.2\% \pm 4.9\%$ with only 100 calibration samples and surpassed 90% with the full dataset. Conversely, subject P4 presented a more challenging adaptation profile. Accuracy remained near baseline (37.3%) at 100 samples, requiring a larger calibration set to bridge the domain gap (60.2% at 1000 samples), eventually reaching $> 83\%$ with full supervision.

This performance disparity suggests that while the adaptation protocol is effective, the sample efficiency is contingent upon the anatomical structure of the user. For subjects sharing biomechanical similarities with the training pool (e.g., P3), a rapid enrollment phase is sufficient to align the pre-learned feature space with the new user's physiology.

V. Conclusion

This work presents a modular NIR optical myography armband that captures gesture-dependent changes in light transport

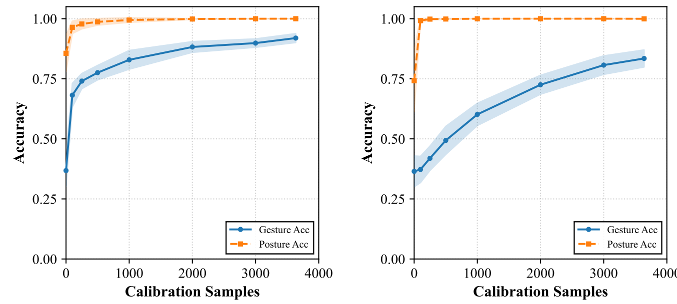

(a) (b)

Fig. 5: Inter-Subject Adaptation curves evaluating the cold start scenario on new users. (a) Target P3 demonstrates rapid alignment with the pre-trained feature space. (b) Target P4 requires a larger calibration set to bridge the anatomical gap.

through forearm tissue. Unlike common wearable systems using reflective phototransistor modules and TIA-based analog front ends, the proposed hardware uses discrete high-power NIR LEDs and silicon PIN photodiodes with charge-integration digitization. This design choice reduces analog front-end complexity, improves sensitivity through temporal integration, and enables digital control of the measurement dynamic range via integration-time scheduling.

Experimental validation on four subjects confirmed that multi-channel optical measurements contain sufficient spatial information to decode fine finger movements, achieving a mixed-subject gesture classification accuracy of $92.5\% \pm 4.6\%$ across four classes and two different forearm postures. A hard-gated multi-task neural architecture separated posture recognition from gesture decoding, delivering near-perfect posture classification and improving robustness to forearm rotation. However, the high spatial selectivity of the optical signal makes the system sensitive to sensor displacement and device repositioning across sessions, which can significantly affect performance. While this spatial selectivity amplifies placement effects, it also enables rapid realignment: a few-shot transfer learning strategy effectively mitigated these shifts and enabled rapid accuracy recovery with minimal user calibration, including for previously unseen subjects. Furthermore, inter-subject results indicate that anatomical variability induces a domain shift in the optical feature space, which can be efficiently compensated through limited user-specific calibration using the same few-shot adaptation framework. A further limitation is the optical measurements' sensitivity to external mechanical perturbations. Although the forearm was left unconstrained, additional contact or pressure on the device can alter sensor–skin coupling and affect light propagation.

Future work will focus on: (i) extending the dataset to a larger and more diverse population, including different genders and skin tones, to better assess generalization and account for inter-subject variability in optical properties; (ii) extending the experimental protocol from static hand gestures to dynamic movements, including continuous transitions between gestures, to better reflect real-world usage scenarios; (iii) hardware and firmware optimization toward lower power operation; (iv) increasing effective optical penetration and channel selectivity through optimized source directionality and collection geometry (e.g., more directive emitters).

Acknowledgment

This work was supported by the Fit4MedRob (Fit for Medical Robotics) project, funded under the Italian National Complementary Plan (PNC).

References

[1] S. B. Rutkove, "Electrical impedance myography: background, current state, and future directions," *Muscle & Nerve: Official Journal of the American Association of Electrodiagnostic Medicine*, vol. 40, no. 6, pp. 936–946, 2009.

[2] R. H. Chowdhury, M. B. Reaz, M. A. B. M. Ali, A. A. Bakar, K. Chellappan, and T. G. Chang, "Surface electromyography signal processing and classification techniques," *Sensors*, vol. 13, no. 9, pp. 12 431–12 466, 2013.

[3] A. S. P. Sousa, A. Noites, R. Vilarinho, and R. Santos, "Long-term electrode–skin impedance variation for electromyographic measurements," *Sensors*, vol. 23, no. 20, 2023.

[4] M. Abdoli-Eramaki, C. Damecour, J. Christenson, and J. Stevenson, "The effect of perspiration on the semg amplitude and power spectrum," *Journal of electromyography and kinesiology : official journal of the International Society of Electrophysiological Kinesiology*, vol. 22, 05 2012.

[5] N. Unanyan and A. Belov, "Case study: Influence of muscle fatigue and perspiration on the recognition of the emg signal," *Advances in Systems Science and Applications*, vol. 21, pp. 58–70, 06 2021.

[6] L. Hargrove, K. Englehart, and B. Hudgins, "A training strategy to reduce classification degradation due to electrode displacements in pattern recognition based myoelectric control," *Biomedical Signal Processing and Control - BIOMED SIGNAL PROCESS CONTROL*, vol. 3, pp. 175–180, 04 2008.

[7] S. Lee and G. Saridis, "The control of a prosthetic arm by EMG pattern recognition," *IEEE Transactions on Automatic Control*, vol. 29, no. 4, pp. 290–302, Apr. 1984.

[8] F. S. Botros, A. Phinyomark, and E. J. Scheme, "Electromyography-Based Gesture Recognition: Is It Time to Change Focus From the Forearm to the Wrist?" *IEEE Transactions on Industrial Informatics*, vol. 18, no. 1, pp. 174–184, Jan. 2022.

[9] J. He, X. Niu, P. Zhao, C. Lin, and N. Jiang, "From Forearm to Wrist: Deep Learning for Surface Electromyography-Based Gesture Recognition," *IEEE Transactions on Neural Systems and Rehabilitation Engineering*, vol. 32, pp. 102–111, 2024.

[10] S. Jiang, P. Kang, X. Song, B. P. Lo, and P. B. Shull, "Emerging Wearable Interfaces and Algorithms for Hand Gesture Recognition: A Survey," *IEEE Reviews in Biomedical Engineering*, vol. 15, pp. 85–102, 2022.

[11] H. Zhou and G. Alici, "Non-Invasive Human-Machine Interface (HMI) Systems With Hybrid On-Body Sensors for Controlling Upper-Limb Prosthesis: A Review," *IEEE Sensors Journal*, vol. 22, no. 11, pp. 10 292–10 307, Jun. 2022.

[12] N. Akhlaghi, C. A. Baker, M. Lahlou, H. Zafar, K. G. Murthy, H. S. Rangwala, J. Kosecka, W. M. Joiner, J. J. Pancrazio, and S. Sikdar, "Real-Time Classification of Hand Motions Using Ultrasound Imaging of Forearm Muscles," *IEEE Transactions on Biomedical Engineering*, vol. 63, no. 8, pp. 1687–1698, Aug. 2016.

[13] S. M. Engdahl, S. A. Acuña, E. L. King, A. Bashatah, and S. Sikdar, "First Demonstration of Functional Task Performance Using a Sonomyographic Prosthesis: A Case Study," *Frontiers in Bioengineering and Biotechnology*, vol. 10, May 2022.

[14] V. Nazari, Y.-P. Zheng, V. Nazari, and Y.-P. Zheng, "Controlling Upper Limb Prostheses Using Sonomyography (SMG): A Review," *Sensors*, vol. 23, no. 4, Feb. 2023.

[15] S. M. Engdahl, S. A. Acuña, R. R. Kaliki, and S. Sikdar, "Sonomyography for Control of Upper-Limb Prostheses: Current State and Future Directions," *JPO: Journal of Prosthetics and Orthotics*, vol. 36, no. 3, p. 174, Jul. 2024.

[16] A. Radmand, E. Scheme, and K. Englehart, "High-density force myography: A possible alternative for upper-limb prosthetic control," *Journal of Rehabilitation Research and Development*, vol. 53, no. 4, pp. 443–456, 2016.

[17] Z. G. Xiao and C. Menon, "A Review of Force Myography Research and Development," *Sensors*, vol. 19, no. 20, p. 4557, Jan. 2019.

[18] E. Fujiwara and C. K. Suzuki, "Optical fiber force myography sensor for identification of hand postures," *Journal of Sensors*, vol. 2018, no. 1, p. 8940373, 2018.

[19] M. K. Gomes, W. H. A. da Silva, A. Ribas Neto, J. Fajardo, E. Rohmer, and E. Fujiwara, "Detection of hand poses with a single-channel optical fiber force myography sensor: A proof-of-concept study," *Automation*, vol. 3, no. 4, pp. 622–632, 2022.

[20] K. Foteinos, J. Cani, M. Linardakis, P. Radoglou Grammatikis, V. Argyriou, P. Sarigiannidis, I. Varlamis, and G. Papadopoulos, "Visual hand gesture recognition with deep learning: A comprehensive review of methods, datasets, challenges and future research directions," *arXiv preprint arXiv:2507.04465*, 2025.

[21] Y. T. Wu, E. Fujiwara, and C. K. Suzuki, "Evaluation of Optical Myography Sensor as Predictor of Hand Postures," *IEEE Sensors Journal*, vol. 19, no. 13, pp. 5299–5306, Jul. 2019.

[22] C. Ash, M. Dubec, K. Donne, and T. Bashford, "Effect of wavelength and beam width on penetration in light-tissue interaction using computational methods," *Lasers in Medical Science*, vol. 32, no. 8, pp. 1909–1918, 2017.

[23] M. Padalkar and N. Pleshko, "Wavelength-Dependent Penetration Depth of Near Infrared Radiation into Cartilage," *The Analyst*, vol. 140, no. 7, pp. 2093–2100, Apr. 2015.

[24] J. McIntosh, A. Marzo, and M. Fraser, "SensIR: Detecting Hand Gestures with a Wearable Bracelet using Infrared Transmission and Reflection," in *Proceedings of the 30th Annual ACM Symposium on User Interface Software and Technology*, ser. UIST '17. New York, NY, USA: Association for Computing Machinery, Oct. 2017, pp. 593–597.

[25] T. Bianchi, D. Zambarbieri, G. Beltrami, and G. Verni, "NIRS monitoring of muscle contraction to control a prosthetic device," in *Biomedical Sensors, Fibers, and Optical Delivery Systems*, vol. 3570. SPIE, Jan. 1999, pp. 157–163.

[26] W. Guo, P. Yao, X. Sheng, D. Zhang, and X. Zhu, "An enhanced human-computer interface based on simultaneous sEMG and NIRS for prostheses control," in *2014 IEEE International Conference on Information and Automation (ICIA)*, Jul. 2014, pp. 204–207.

[27] W. Guo, X. Sheng, H. Liu, and X. Zhu, "Toward an Enhanced Human–Machine Interface for Upper-Limb Prosthesis Control With Combined EMG and NIRS Signals," *IEEE Transactions on Human-Machine Systems*, vol. 47, no. 4, pp. 564–575, Aug. 2017.

[28] E. Tamaki, S. Hosono, and K. Iwasaki, "Firstvr: A muscle deformation sensors array device to detect finger gestures and noise reduction case," in *Proceedings of the 2019 2nd International Conference on Electronics, Communications and Control Engineering*, ser. ICECC '19. New York, NY, USA: Association for Computing Machinery, 2019, p. 21–24.

[29] H. H. Muhammed and J. Raghavendra, "Optomyography (omg): A novel technique for the detection of muscle surface displacement using photoelectric sensors," in *Proceedings of the 10th International Conference on Bioelectromagnetism (ISBEM)*. International Society for Bioelectromagnetism, 2015.

[30] A. Maereg, Y. Lou, E. L. Secco, and R. King, "Hand Gesture Recognition Based on Near-Infrared Sensing Wristband," in *4th International Conference on Human Computer Interaction Theory and Applications*, Malta, Dec. 2019.

[31] A. Dahiya, R. Katti, and L. G. Occhipinti, "Real-Time Hand Gesture Classification Using Infrared Sensor Arrays-Based Wearable Bracelet and Efficient 1-D Convolutional Neural Network," *IEEE Sensors Letters*, vol. 9, no. 6, pp. 1–4, Jun. 2025.